Enhancement of metal adhesion thanks to the plasma texturing of PEEK

David Gravis, Grégoire Rigolé, Mayssa Yengui, Wolfgang Knapp, Jean-François Coulon, Fabienne Poncin-Epaillard

Article type: Original Article

Enhancement of metal adhesion thanks to the plasma texturing of PEEK

David Gravis[1,2], Grégoire Rigolé[1], Mayssa Yengui[1], Wolfgang Knapp[3], Jean-François Coulon[1,2], Fabienne Poncin-Epaillard[2*].

[1] ECAM RENNES - Louis de Broglie, Campus de Ker Lann, CS 29 128, 35091 Rennes Cedex 09, France

[2] Institut des Molécules et Matériaux du Mans, Le Mans Université - CNRS n°6283, Avenue Olivier Messiaen, 72085 Le Mans, France

[3] IMN - POLYTECH, Université de Nantes, Site de la Chantrerie, Rue Christian Pauc, 44306 Nantes cedex 3, France

*Correspondence

Fabienne Poncin-Epaillard, Institut des Molécules et Matériaux du Mans, Le Mans Université - CNRS n°6283, Avenue Olivier Messiaen, 72085 Le Mans, France

Email: Fabienne.poncin-epaillard@univ-lemans.fr

Abstract. To understand both chemical and anchoring aspects of Al adhesion, the PEEK surface was plasma textured prior to be coated. The practical adhesion was compared to that obtained by laser texturing. The surfaces and assemblies were characterized by SEM, AFM microscopies, surface free energy determination and pull-off tests. Patterning processes increase the Al adhesion. O_2 plasma appears to be the most efficient through a texture assigned to the chemical erosion while Ar plasma mostly induces material etching with

thermal effects altering the PEEK crystallinity. With low pressure plasmas, this texturing can be added to the chemical functionalization in order to further increase the adhesion.

Keywords: aluminum - PEEK assembly; laser; plasma; texturing

1 INTRODUCTION

Improving the adhesion of polymer substrates requires a modification of their surface properties. Numerous methods are commonly used in industry, some of them allow a surface functionalization by a chemical modification; the creation of new chemical bonds for thermodynamic adhesion is therefore favored. Other methods also alter the texture or the surface roughness to promote mechanical anchoring, by increasing the real contact area of the material with the adherent.[1,2] In fact, most surface chemical modification processes are accompanied by an alteration in roughness which is certainly minor, so that the grinding process used to increase the adhesion potential may also change the chemical surface composition. The increased roughness can be easily obtained at reduced cost by mechanical abrasion (grinding, sanding or sandblasting) but may be relatively ineffective and hard to control.[4] Chemical methods are also described, such as acid etching,[5] but are sometimes accompanied by an alteration of the physicochemistry of the surface and the etching in solution requires the use of solvents which are themselves toxic and sometimes volatile (VOC).

Laser ablation in continuous or pulsed mode allows very precise control of the topography and does not require solvents. Although there are many examples of laser treatment allowing chemical modification in the presence of a gas,[6–9] the main purpose of ablation is to modify the topography of the surface by localized vaporization of the material. The first treatments of organic matrices by irradiation with a UV laser were published in the 1980s.[10,11] Taking into account the material absorption coefficient,[12] the treated area of the

material is of the order of several multiple wavelengths.[13–15] It is thus possible to precisely control the ablation depth by the exposure time or the number of pulses.[16,17] However, ablation requires to take into account the polymer absorption coefficient at the laser wavelength, this often requires adding an absorbing chemical group or molecule.[18,19] There are two modes of laser-matter interaction depending on the mechanism of bond scission: photochemical mode (homolytic scission) and photothermal mode with lasers having wavelength greater than the polymer absorption.[13,14,20] This latter case causes a local increase in the surface temperature inducing the texture.[16] These drawbacks of fusion or swelling with the using of IR lasers can be avoided thanks to the pulsed mode (≈ 1 - 100 ps) in which the ablated matter is vaporized within a few picoseconds.[13,14,21-24] The reduction in the pulse duration thus allows a more efficient and better resolved ablation of the PEEK.[14,25] The increase in adhesion thanks to laser texturing has already been reported to increase the contact area between the coating and the substrate or to allow filling of the structure and to promote the mechanical anchoring.[26,27–29] The most studied structure in the literature, due to its simplicity of implementation, is based on an orthogonal mesh (squares, crossed lines, etc.).[30,31] With a view forming a denser and more isotropic structure, a hexagonal periodic structure is better designated with circular laser impacts.[32] However, few publications show an in-depth study of the influence of the characteristics of the textured surface on the adhesion properties, due to the complexity and the number of geometric and mechanical parameters on which it depends.[26]

Low pressure plasmas combine the reactions of activated neutral species and the interactions of ions with matter, the latter inducing the transfer of energy which can lead to sputtering of the matter. The ions can then be used as vectors for the texturing of the surface, which is combined with the chemical functionalization by the activated neutrals. The kinetic energy of the incident ions is critical to allow this erosion and depend on the mean free path of the ionized particle, and therefore on the pressure.[33-38] It is also necessary to take into

account the localization of the treated surface in the chamber,[39,40] which influences the sputtering rate. The texture can also be formed by a preferential chemical erosion of the amorphous zones, which is reported to be more effective in the case of O_2 plasmas.[4,40–43] The preferential chemical degradation of the amorphous zones allows etching of these parts while the crystalline phases remain partially un-etched leading to the creation of a texture of the surface.[42–44] The etched amorphous material is ejected from the surface either by physical ion bombardment, or by induced oxidation leading to volatile compounds;[45] the damaged amorphous part of the material can also diffuse up to the crystalline zones serving as a germ of crystallization.[41,46] In the case of the chemical etching with an O_2 plasma, the etching speed is dependent on the concentration of $O^{\bullet}$ radicals. The injection of gaseous additives increasing the plasma ionization rate, and therefore ultimately the atomic oxygen concentration, further promotes this etching.[40,41] Increasing the exposure time and the power dissipated in the plasma phase increases the surface roughness and the size of the textured structures.[47–51] Nevertheless, the random aspect of the texturing (although isotropic and uniform) does not allow to deepen the analysis of the geometry of the texture. However, this roughness is often identified as favorable to the adhesion, and some studies report on the additional effect of this texturing to that of the chemical functionalization on the mechanical strength of an assembly.[48]

In our previous work,[52] the effects of the chemical functionalization thanks to plasma processes have been highlighted. More specifically, the plasma chemistry under atmospheric pressure and under low pressure plasmas provides a surface chemistry enhancing the adhesion of the metallic coating on the PEEK substrate. Here, the aim of this study is to correlate both the surface chemistry and the texturing with the adhesion properties of Al - PEEK assembly in the case of the low pressure plasma. The morphological pattern was prepared through the plasma process itself and then compared to the laser process; both effects are studied in terms of adhesion after the deposition of an aluminum thin layer obtained by thermal evaporation.

2 EXPERIMENTAL SECTION

2.1 Materials and sample preparation

Victrex® 450G PEEK foils of 50 × 25 × 5 mm were prepared for the measurement of the practical adhesion strengths, while 50 × 15 × 5 mm samples were used for the surface free energy measurements. All the surfaces were polished with a Struers LaboPol-5 polishing machine, using silicon-carbide papers with a steady decrease in grain size (from 150 to 4000). The samples were washed in an ultrasonic bath with ethanol for 30 min before surface treatment.

2.2 Plasma surface and laser treatments

Two plasma treatments were used to compare their respective efficiency and to check the possible texturing mechanisms they could have in common: an atmospheric pressure plasma treatment and a low pressure plasma treatment. An atmospheric cold plasma treatment was applied using the Ultra-Light System arc plasma torch from AcXys™; in this system, the plasma (dry air, 4 bar) is sustained by a high voltage (1.5 kV) and low frequency power (100 kHz). The treatments were conducted by varying the scan speed (from 10 to 100 mm/s), the number of scans (1, 2 and 3) and the surface – plasma distance (2, 3, 4 cm). Further information on the parametric study of this plasma apparatus can be found in our previous work.[52] Vacuum plasma treatments were conducted in a cylindrical stainless steel plasma chamber of internal dimensions of 32 cm in diameter and 24 cm in height (average volume of 19 L). A pumping system consisting of a primary pump and a turbo-molecular pump (Alcatel Adixen ATH 300) was used. Two gas inlets allow the injection of gas mixtures (Table 1) selected between argon, dinitrogen and dioxygen, and controlled by flow meters; a constant total flow rate of 10 sccm was used for all the experiments, while respective flows were varied from 0 to 10 with a 2 sccm step, and the 50/50% composition. The working pressure was measured by a capacitive gauge (Pfeiffer CCR364) and maintained between 0.2 and 1.5 Pa. The plasma was created through 12 microwave antennas, each of them ending with a dipole magnet that ensures the electron cyclotron resonance (ECR) coupling at microwave (2.45 GHz) frequency. The distance between two diametrically opposed magnets was fixed at 20 cm. The applicators were uniformly distributed on the wall of the plasma chamber and individually powered by a microwave generator (Sairem GMP20KED) via a divider guide; dissipated powers in the range of 500 - 1500 W were studied, with a 250 W step. Each

applicator was provided with an impedance matcher meant to reduce the reflected power. The microwave applicators, the plasma chamber walls and the substrate holder were water-cooled. The substrate holder allowed a free positioning of the substrate, for distances between the surfaces and the plasma glow of 0, 6 and 12 cm. Surfaces were treated during 5 or 10 min.

The laser texturing of the surfaces was carried out in cooperation with an industrial partner, Industrial Laser Systems (Vanves, France), using a femtosecond infrared laser PHAROS Light Conversion Yb:KGW [$KGd(WO_4)_2$ crystal doped with Yb^{+3}] with a wavelength λ = 1026 nm, pulses duration of 224 fs, with an average power varying from 1 to 10 W. The repetition rate is between 50 and 610 kHz. The laser spot with a Gaussian profile of 40 µm in diameter is moved over the surface using a set of movable lenses. The texture of hexagonal geometry was produced on a surface of 25 x 25 mm. After texturing, the samples were cleaned in ethanol ultrasonic bath for 30 min to remove residues.

2.3 Metallic thin films deposition

Aluminum thin films were grown on the polymer surfaces by thermal evaporation, using an Alcatel thermal evaporator chamber. The residual pressure before deposition was $5\ 10^{-6}$ mbar, and rose to 10^{-5} mbar during film growth. 1 µm thick films of metal was deposited onto PEEK substrates.

2.4 Wettability and surface energy

The contact angle (CA) measurements were performed with the sessile drop method to determine the wettability of the surface and to quantify the surface energy, calculated by the Owens-Wendt method.[53] This method is based on the measurement of static CA for different liquids, from which the dispersive and polar components of the surface energy are calculated. Water and diiodomethane were used as polar and non-polar liquids, respectively (Table 1).

TABLE 1. Surface free energy of the liquid probes.

	γ [mJ.m^{-2}]	γ_p [mJ.m^{-2}]	γ_d [mJ.m^{-2}]
Water	72.8	51.0	21.8
Diiodomethane	50.8	0	50.8

Drops of 3 µl of both liquids were placed on the surfaces of the samples. The pictures of the droplets were captured with a numeric camera coupled to an optical microscope. The

contact angles (θ) were calculated based on the measurement of the diameter (D) and height (h) of the droplets according to the following equation (eq 1):

$$\theta = \arctan\left(\frac{2h}{D}\right) \quad \text{(eq 1)}$$

This measurement method was chosen to lower the standard deviation induced by asymmetrical droplets, and to attain a higher precision than for direct angle measurements especially for small values of contact angles. The average values of *h* and *D* for 10 drops were used; the surface energy standard deviations were derived from the standard deviations of the CA measurements, for which the dispersion range was chosen to remain < 2 °.

2.5 Profilometry

A KLA Tencor D-120 profilometer was used for surface profile measurements. Depending on the required resolution for the acquisition of significant profiles, two different mechanical probe were used: one with a radius of curvature of 12.5 µm (tip angle of 60 °), and a tip of 2 µm with radius of curvature (45 ° tip angle). A force of 5 mg was used for the 12.5 µm radius tip, while a force of 1 mg was used for the second. The profiles were measured with 0.03 mm / s speed for lengths between 1 and 5 mm. Under such conditions, the vertical resolution is about 1 nm and lateral resolution about 0.4 µm. The acquisition of 3 concordant results were carried out to obtain significant results.

2.6 SEM and AFM microscopies

The Hitachi S3200N scanning electron microscope was used in secondary electron imaging mode with an acceleration voltage of 20 keV. The insulating nature of the PEEK material was countered by a metallization obtained by sputtering with a gold-palladium coating 10 nm thick. An additional conductive jumper between the metallized surface and the sample holder (grounded) was provided by silver lacquer.

The AFM apparatus is a Multimode 8 Bruker machine. AFM images were recorded on samples whose dimensions 1x1 cm and a thickness of approximately 2mm. The length of the cantilever is 115 µm. The oscillation frequency of the tip used is F_0 = 70 kHz and the elasticity constant is k = 0.4N / m. The results were processed using WSxM software used for AFM image processing. Two types of roughness are determined: The first one is the *RMS* (Root mean square, eq 2) roughness:

$$RMS = \sqrt{\frac{1*\sum_{i,j}(a_{i,j}-<a>)^2}{N}} \quad \text{(eq 2)}$$

With *N*: the surface analyzed, $a_{i,j}$: the height of each measured point, <*a*>: the average height of the peaks on the surface. The second one is the *Sa* roughness calculated as follows in eq 3:

$$Sa = \frac{\sum_{i,j} |a_{i,j} - \langle a \rangle|}{N} \quad \text{(eq 3)}$$

2.7 Pull-off tests

The pull-off test method was used to characterize the adhesion of thin metallic films on polymer surfaces; in this study, 1 µm aluminum thin films were grown on the polymer surfaces by thermal evaporation (Alcatel thermal evaporator chamber). The pull off test allows a reproducible and relative study of adhesion stresses if one takes several experimental precautions, as previously reported.[54–56] The measurements of practical adhesion stresses (σ_{adh}) were performed with an Instron 4204 tensile strength system under a constant speed of 2 mm / min, by using 2 cm-diameter aluminum dollies glued to the metallic thin films with an epoxy resin (Araldite 2011). In this study, statistical quantification of the adhesion stress was ensured with the measurement of tensile strengths for four to six individual measurements.

3 RESULTS AND DISCUSSION

~~In our previous work,[45] the effects of the chemical functionalization thanks to plasma processes have been highlighted. More specifically, the plasma chemistry under atmospheric pressure and under low pressure plasmas provides a surface chemistry enhancing the adhesion of the metallic coating on the PEEK substrate. Here, the aim of this study is to correlate both the surface chemistry and the texturing with the adhesion properties of Al - PEEK assembly in the case of the low pressure plasma. The morphological pattern was prepared through the plasma process itself and then compared to the laser process; both effects are studied in terms of adhesion after the deposition of an aluminum thin layer obtained by thermal evaporation~~.

3.1 Aluminum adhesion on the reference sample: the laser-textured PEEK

To determine the influence of a texture on the adhesion properties, the study was focused on the effect of different geometric patterns on the adhesion stresses of Al thin metallic layers. Such geometries are defined by etched lines distributed over the surface. But for a better comprehensive purpose, static and dynamic ablation of polymeric material was studied. A systematic analysis of the influence of the power, the number of shots and their frequency on the geometry of the etched surface was therefore carried out as illustrated in Figure 1.

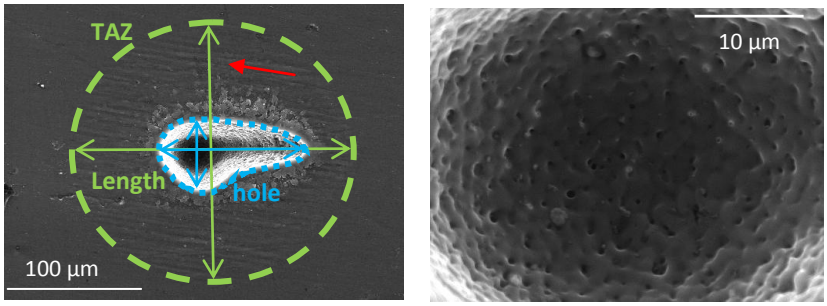

a) *b)*

FIGURE 1. Laser impact on PEEK (*P* = 5 W, *v* = 50 kHz) a) 1 shot (x400), b) 2 shots (x3000)

The laser texturing of PEEK leads to the appearance of holes with an ellipsoid asymmetrical shape explained by the optical path of the infrared beam (Figure 1a). Whatever the laser parameters are, the average size of the holes is around 40 µm in the plane of the surface with a mean depth of about 30 µm. The inner walls of the holes show a random secondary texture (Figure 1b) whose morphology is independent of the laser parameters and should be in favor of the Al mechanical anchoring. This random secondary structure is due either to the disturbance of the laser beam caused by impurities present in the polymer bulk such as fillers or residues of catalyst, whose absorptions are different from that of the matrix, or by recrystallization phenomena following a local fusion near the laser impact.[57] Indeed, an infrared laser always induces thermal phenomena altering the resolution of the etching[58] and leading to a diffused area near the hole, so-called thermal-altered zone (TAZ) (represented by the outer dashed green circle, Figure 1a) composed of ripples (arrow on Figure 1a) due to the polymer absorption at the wavelength corresponding to the IR range.[22] The parametric study (cf Figure 1, supporting information) gave evidence of the increase of hole and TAZ dimensions with the increase of laser power whatever the number of shots at fixed pulse frequency. However, increasing the pulse frequency decreases the TAZ length assigned to a less thermal absorption and a more important photochemical effect.[25,59]

Successive and overlapping laser shots induce the linear etching of PEEK and the appearance of a rough surface at the bottom of the holes assigned to redeposit phenomena of the etched polymer or to the creep behavior of the melted material (Figure 2). This corresponds to the double scale texturing observed in static mode which could enhance the Al adhesion. The power increase induces an increase in the dimensions (width and depth) of the lines, by increasing the amount of etched material. Increasing the spatial distance of successive laser pulses decreases these dimensions, with a more marked effect on the depth of the line. The overlap of shots therefore has very little influence on the width of the ablated

area, but allows the erosion of more material per area unit. Details are given in the supporting information (Figures 2,3).

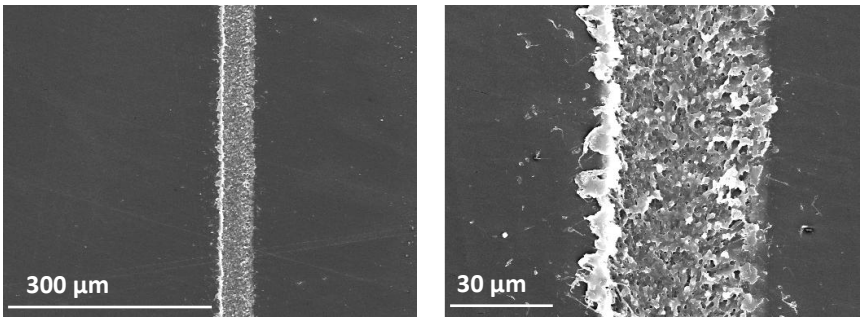

a) b)

FIGURE 2. SEM pictures (a) x200; b) x1000) of etched lines (P = 2 W, v = 100 kHz and d = 5 µm)

The texture defined for a convenient Al adhesion study was chosen as an equilateral triangle. Such a choice is justified by the possible elaboration of a large range of texture density per unit area. The symmetry order of the equilateral triangle limits the effects of anisotropy which could induce a directionality of the structure like observed with the so-called rice leaf effect.[60,61] Such pattern is obtained by crossing the lines at an angle of 60 °. The dimensions of these triangles are defined by the length of their edges (L), which is the result of the distance separating two parallel lines. The effect of the number of shots (d) within the same line is also studied and illustrated in Figure 3.

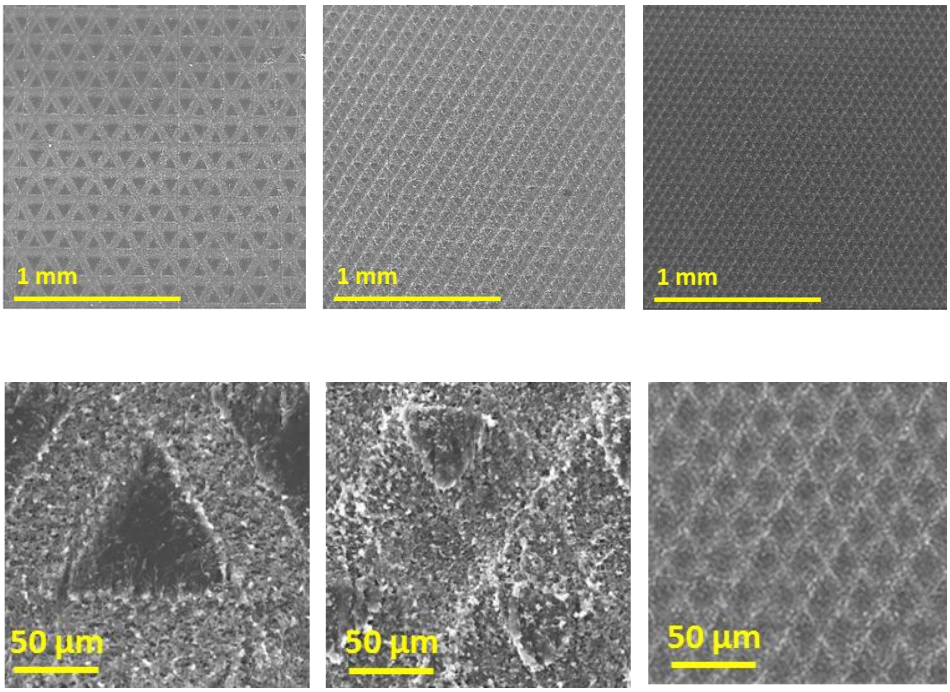

FIGURE 3. SEM pictures of triangular textures x50 (top); x200 (down), left: L = 180 µm; middle: L = 100 µm; right: L= 60 µm (P = 5 W, d = 10)

The obtained patterns (equilateral triangles) are isotropic. Their etching carried out thanks to the crossing of lines also gives rise to double-scale morphology at the bottom of the ablated lines, but also along the edges, as observed previously. An increase in the density of shots along the line, or in the number of patterns per surface area promotes the appearance of this rough morphology. A too large reduction in the pattern size results in the disappearance of the triangle geometric texture, in favor of a total and uniform coverage of the surface by the random secondary texture (Figure 4a). Indeed, in this case, increasing the power induces an increase of the roughness. While this effect should be beneficial for the adhesion, the opposite behavior is observed as the practical adhesion stress decreases. This implies that the random secondary structure could degrade the practical adhesion when it is predominant on the surface (Figure 4).

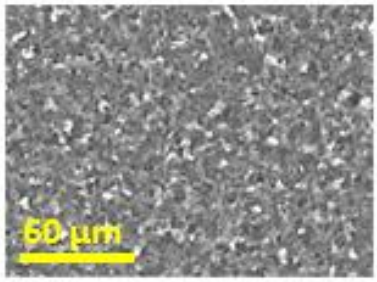

a)

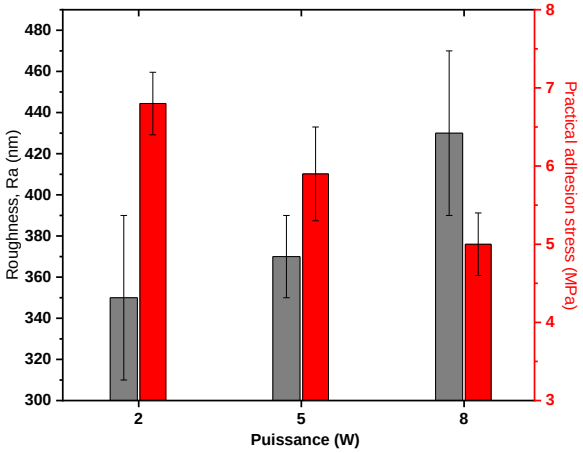

b)

FIGURE 4. The secondary random structure. (a): SEM photograph. (b): dependence of the roughness and the practical adhesion stress on the laser power for PEEK surface when it is completely covered by the secondary random structure

The influence of the combined defined geometric texture and the random secondary structure is analyzed versus the adhesion of Al coatings (Figure 5).

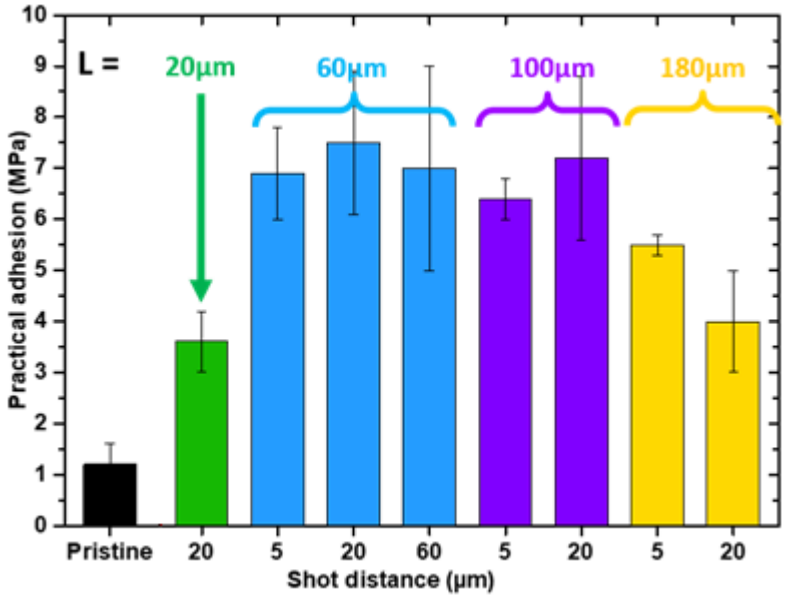

FIGURE 5. Dependence of the practical adhesion stress on the dimensions (*L*, *d*) of the pattern geometry

The practical adhesion stress increases from 1.2 ± 0.4 MPa (pristine PEEK) to values between 3.6 ± 0.6 and 7.5 ± 1.4 MPa respectively for L = 20 µm, d = 20 µm and L = 60 µm, d = 20 µm. Triangular patterns whose sides measure 60 µm have been found to be the optimal values for increasing the Al adhesion. The variation in the distance between shots does not give a significant variation in the adhesion stresses. As the triangle side is increasing above 60 µm, one can observe that the practical adhesion stress is less improved and even strongly decreases with L = 180 µm. We assumed this decreasing to be correlated to the lower density of the texturing, arguing for an optimal geometry with L = 60 µm. The contribution of the random secondary structure in this increase is not possible to be highlighted and cannot be separated from the role of the triangle well defined geometry. It is therefore difficult to interpret these variations as compared to simple geometric considerations, where only the triangles size would be taken into account. No consideration of the surface, in the three dimensions, has been made so far. This is why a specific surface calculation (cf supporting information) was carried out to take into account the variations of the depth of the ablated areas, but also the density of the patterns, by the variation of the relative scales of the different textured triangles. The dependence of the practical adhesion stress on the ratio between the apparent and developed surfaces (*R*) is given in Figure 6.

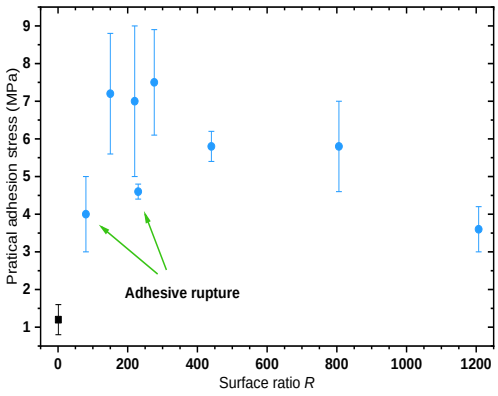

FIGURE 6. Dependence of the practical adhesion stress on the developed and apparent surfaces ratio (blank with R = 1: black dot)

The practical adhesion stress thus increases from 4.0 ± 1.0 MPa to 7.5 ± 1.4 MPa for R varying from 80 to 280, and then decreases down to 3.6 ± 0.6 MPa for R of about 1200. Only two texturing conditions presented an adhesive failure mode (triangles of 180 µm, practical adhesion measured of 4.0 ± 1.0 and 4.6 ± 0, 2 MPa). All the other samples showed a cohesive failure mode in the PEEK substrate, for a larger surface ratio, whatever the measured adhesion stresses. An increase in R implies an increase of the roughness in favor of the mechanical anchoring as already reported;[8,28,62] the adhesion stress increases very quickly with R, up to values of R of approximately 300. The mode of rupture also evolves quickly towards a cohesive mode within the substrate. Beyond R = 400, the adhesion stress decreases suggesting the alteration of the mechanical strength of the assembly. Several hypotheses could explain such a behavior: (i) thermal degradation during laser irradiation as well as appearance of random secondary structure; (ii) material etching and redepositing leading to the appearance of weak boundary layer weakening the assembly interface; (iii) roughness increase altering the constraints' dissipation to the bulk leading to its rupture. Although these three phenomena are concomitant, the formation of the weak boundary layer in the case of a too dense secondary texture seems the most probable cause.

3.2 Aluminum adhesion on the plasma-textured PEEK

Compared to the laser-texturing, the plasma treatment in a one-step process allows preparing textured surfaces with a controlled surface chemistry.[63,64] Such double treatment is possible with a low pressure ECR plasma by subjecting the surface to a flow of activated neutral species allowing the modification of the chemistry, and to a flow of ions allowing the

texturing. The ionic bombardment is enhanced when an external bias voltage is applied onto the substrate whatever the plasma composition (Figure 7).

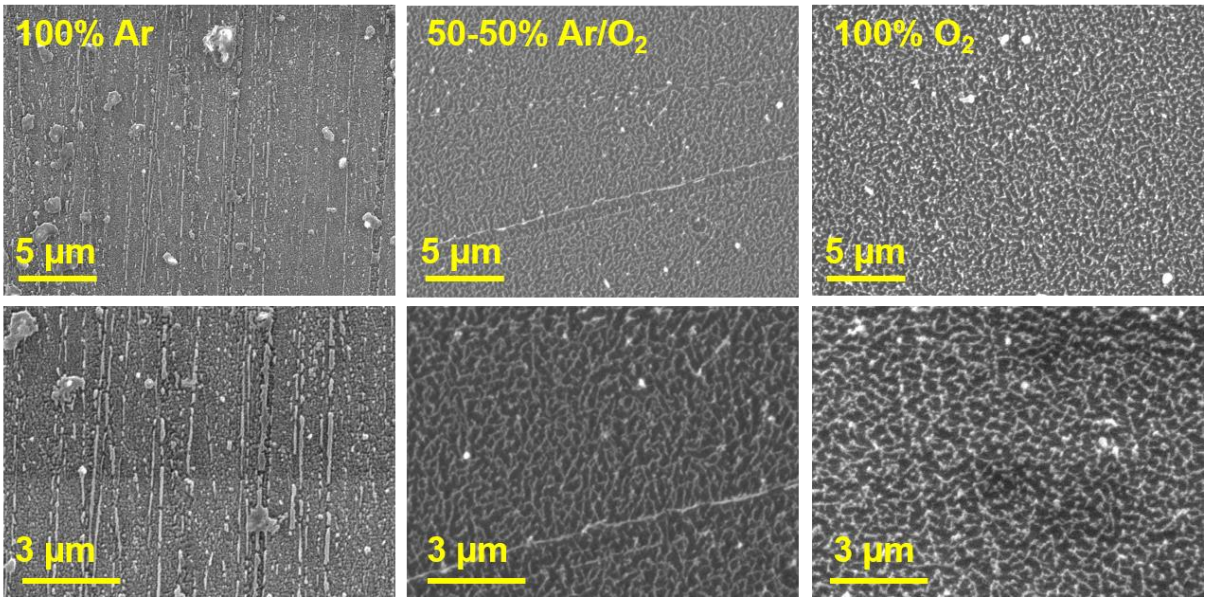

FIGURE 7. SEM pictures (respectively top x500 and down x1000) of plasma-textured surfaces versus the gas phase, pure Ar (left), pure O_2 (right) and 50/50 Ar/O_2 (middle). Plasma conditions are: P = 1500 W, d = 0 cm, t = 15 min, U_s = -200 V.

Two types of structures are obtained under the substrate polarization, depending on the gas composition. In pure Ar plasma, the structures are similar to ripples; but adding dioxygen to the gas mixture induces the appearance of a more isotropic morphology. The different patterns are partially explained by the plasma properties themselves. Indeed, a pure Ar plasma is denser in ions, mainly reinforcing the effect of pulverization. Moreover, the ionic interactions with the surface also induces an increase in the temperature and consequently local fusion of crystallites that diffuses nearby, until the appearance of linear features whose form is originated from polymer processing history. With oxidizing plasma whatever the O_2 concentration, the obtained pattern is composed of fine islet structures of sizes comprised between a few tens and a few hundreds of nm, as already reported in.[47] Since these plasmas are less dense due to lower electronic temperature, the texturing process is mostly assigned to a chemical erosion of the amorphous polymeric zones, and therefore to the retention of surface crystallites.[45,65] Such pathway is also supported by the differences in the chemical

reactivity and the ionic bombardment resistance of the crystalline and amorphous phases.[66,67] The amorphous chains are chemically split and the resulting lower molecular weight degraded and oxidized.[38] oligomers are ejected from the surface under ionic impact. These molecules can also diffuse up to crystalline zones and bind to the crystalline chains thanks to the UV emission of the plasma.[45,46] Furthermore, the morphology of the oxidizing plasma-textured surface and its size show no significant change depending on the applied external bias voltage (cf supporting information, Fig. 5); this means that in such cases the ions are not the prevalent species in the texturing process.

The surface morphology for a plasma treatment containing dinitrogen (Figure 8) is different from the other plasmas and less marked since the isotropic features appear to be smaller. This is explained again by both physical and chemical plasma properties: the ionization rate is greater in N_2 plasma than in O_2 plasma, but nevertheless lower than in Ar plasma.[68,69] therefore even if the ionic bombardment has a limited thermal effect compared with Ar plasma, it cannot be negligible. Besides, evidence of chemical degradation of amorphous zones by N_2 plasma is reported in[46,70] but such surface reaction is less effective than in O_2 plasma.[43,71] So, the N_2 plasma-patterning is resulting in both chemical and / or ionic erosion, but in less effective manner.[65,71–73]

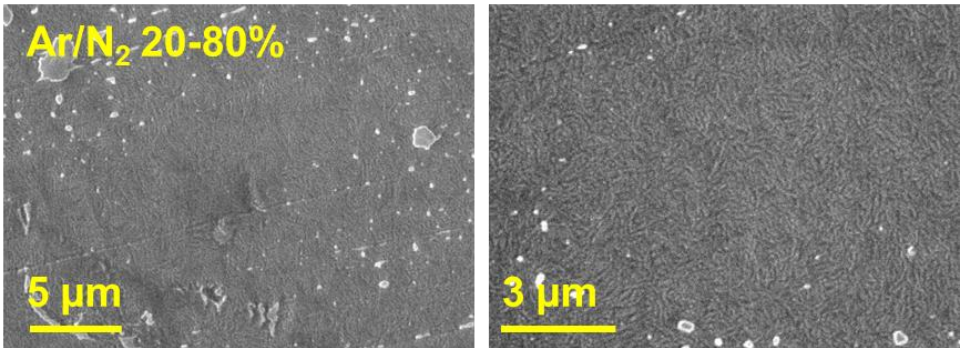

a) b)

FIGURE 8. SEM pictures (respectively a) x10000 and b) x20000) of plasma-textured surfaces (P = 1500 W, d = 0 cm, t = 15 min, U_s = - 200 V, 20-80 % Ar-N_2)

From these observations, one can conclude that Ar plasma-texturing is mainly due to the atomization of matter by ion bombardment; thermal effects induce fusion and surface

rearrangement. With N_2 plasma, an ion bombardment is always noticed, but, however, less intense, limiting thermal phenomena. The chemical degradation of the surface also takes place, preferentially eroding the amorphous phases of the material. O_2 plasmas are not dense enough to be effective as an ion bombardment. The texturing is therefore mainly due to the chemical degradation of the polymer into volatile or diffusing compounds towards the crystalline zones.

Atomic force microscopy reveals the three-dimensions of these features (Figure 9). With pure Ar plasma, the topography of the surface is governed by surface ripples which provide regular lines spaced by 100 nm or 200 nm and up to 100 nm height. With pure dioxygen, the isotropic pattern is thereby well defined as observed by SEM and composed of homogenous but quite separated features of about tens of nm height (Figure 8).

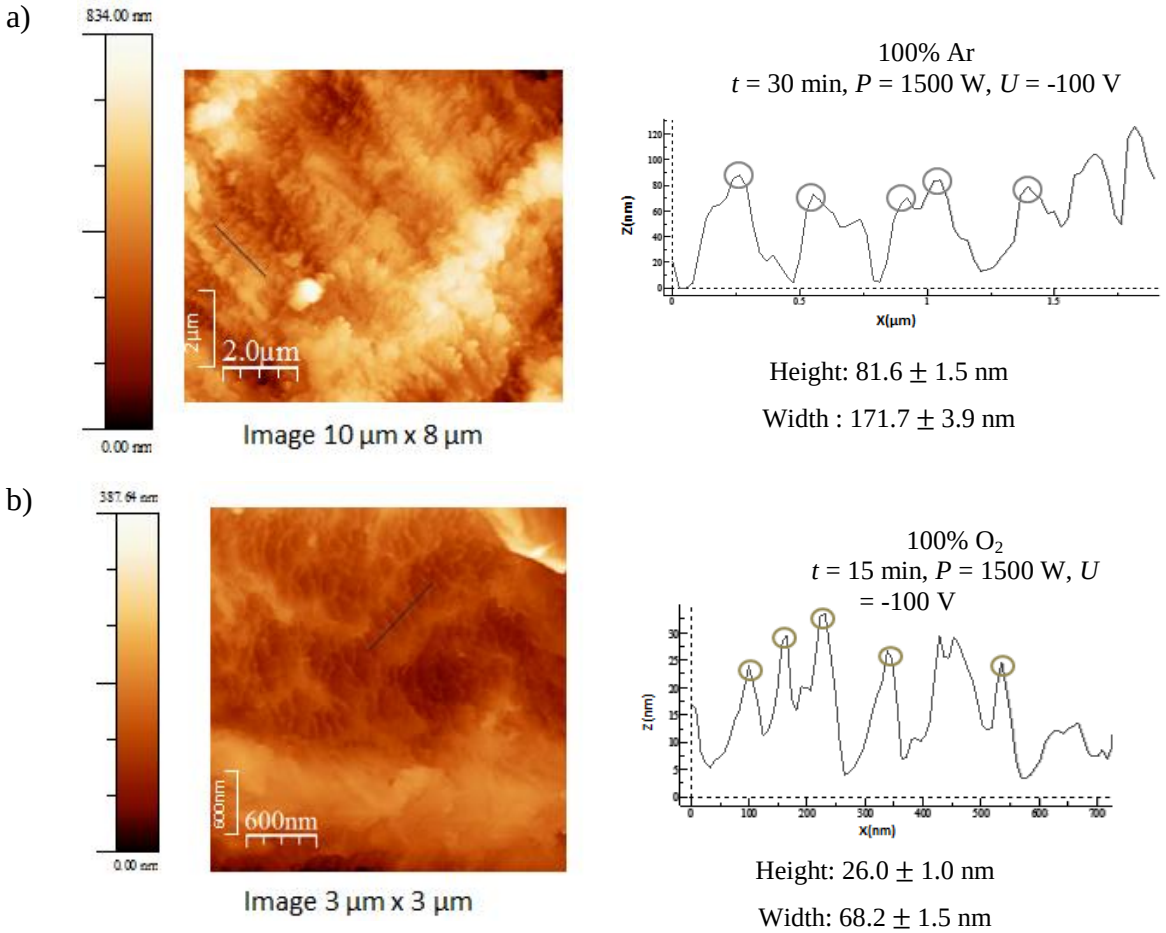

FIGURE 9. AFM images and profiles for a) pure Ar and b) pure O_2 plasma-treated PEEK - Bias voltage of - 100 V

These textured surfaces were covered by Al thin layer and their respective practical adhesion stress determined (Figure 10). The adhesion stress increases from 1.2 (pristine) to

around 5 MPa for pure Ar plasma, and to values close to 8 MPa with the addition of dioxygen. However, the practical adhesion stress does not significantly vary on O_2 proportion in the plasma and on the voltage applied to the substrate. Only a reduction in the stress is observed for increasing bias-voltages in pure Ar atmosphere: it decreases from 5.3 ± 0.6 MPa (-100 V) to 3.8 ± 0.2 MPa (-300 V). The overall evolution is similar to that observed with a smooth plasma-treated surface.[52] However, the practical adhesion stresses measured with textured surfaces are 2 MPa higher than those measured for smooth plasma-treated surfaces, which suggests an improvement in adhesion by mechanical anchoring of the metallic thin layer in the surface structure. Such a decrease with Ar plasma as a function of the external voltage could be explained by the observed fusion phenomena. Indeed, the increase in voltage is accompanied by an increase in the surface temperature and therefore weakening the assembly, as observed for atmospheric plasma.[52] With the high ion density of an Ar plasma, such local fusion and PEEK weakening is emphasized. This could explain why the rupture evolves from the adhesive to cohesive mode, until the rupture of the PEEK when the tension increases.

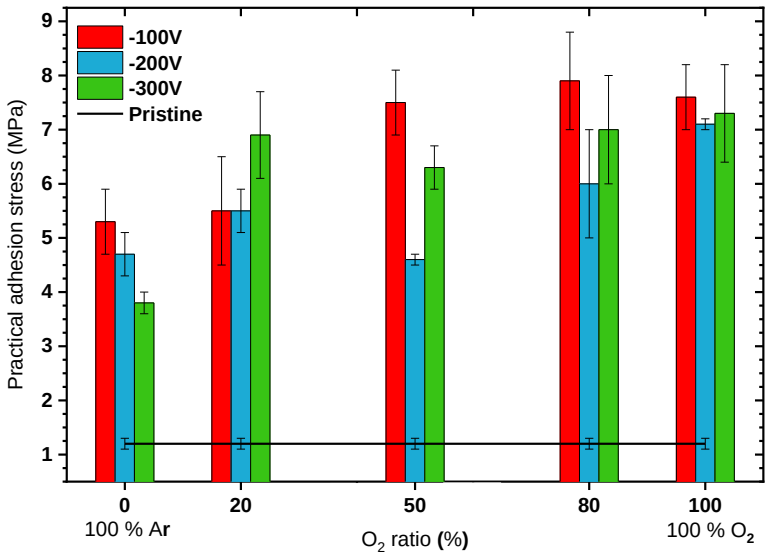

Fig. 10.

FIGURE 10. Dependence of the Al practical adhesion stress on plasma composition (Ar/O_2) and external bias (P = 1500 W, t = 15 min, d = 0 cm)

When adding dioxygen, the cohesive ruptures in the Al layer or in the PEEK matrix are noticed but without obvious link to the experimental conditions. Unlike Ar plasma, the failure mode is not only dependent on the applied voltage probably because of a too low ion bombardment which limits the thermal effects on the surface. Nevertheless, the selective etching of dioxygen leading to the appearance of a weak boundary layer,[4,74,75] local stresses due to the texturing may be also factors reducing the mechanical strength of the assembly.[76]

For the Ar / N_2 plasma-treatment (Figure 11), the practical adhesion stress remains almost constant around 4.5 MPa up to 50% of injected dinitrogen; it then reaches 7 ± 1 MPa in pure N_2 plasma. All the adhesion tests for substrates treated with a mixture of Ar / N_2 showed an adhesive rupture. The increase in the adhesion stress at high dinitrogen concentrations (> 50%) up to 7 MPa, is of the same order of magnitude as the stresses obtained for oxidizing plasmas. This observation is different from the results obtained for low pressure treatments without polarization, where the stress measured was 2 MPa higher for O_2 plasma treatments than for N_2.[52] This was assigned to chemical functionalization by O_2 plasma more favorable to the adhesion than N_2 plasma, through the creation of stronger chemical bonds. Here, since the N_2 plasma-texturing leads to smaller features, the stress concentrations could be reduced, and therefore reduce the risks of material rupture. Cohesive failure with O_2 plasmas would therefore limit the maximum stresses achievable.

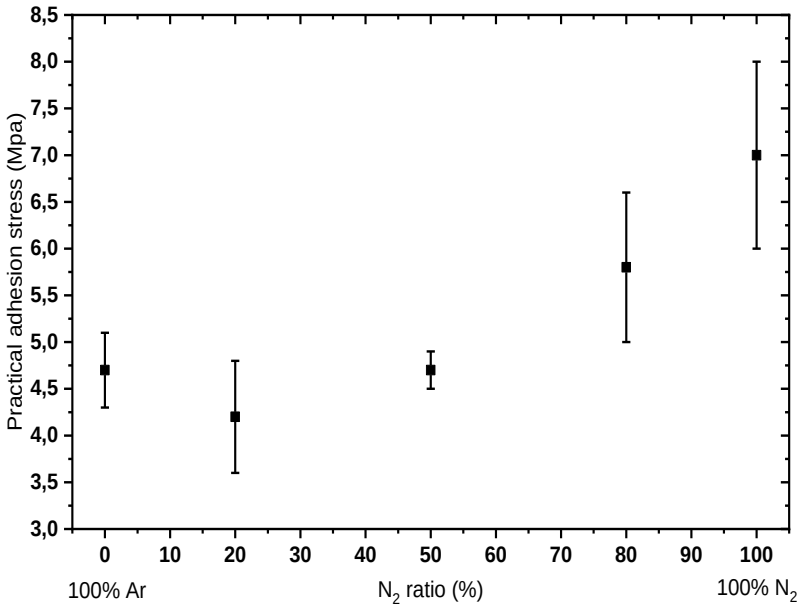

Fig. 11.

FIGURE 11. Dependence of Al practical adhesion stress on N_2 proportion in Ar/N_2 plasma (P = 1500 W, t = 15 min, d = 0 cm, U_s = - 200 V)

3.3 Correlation between the different texturing processes and the aluminum adhesion PEEK

Adhesion between two materials is dependent on several factors such as the surface functional groups and the surface roughness that respectively enhance the appearance of interfacial chemical bonds and mechanical anchoring. Therefore, both properties when added can simultaneously influence the practical adhesion stress. In order to illustrate their respective effect, the effect of the chemical functional groups created on PEEK with atmospheric plasma or ECR plasma treatments is fully described in [52] and in these examples no roughness and texturing were noticed. Figure 12 reports the results of this previous study completed with those of the texturing ECR plasma treatment.

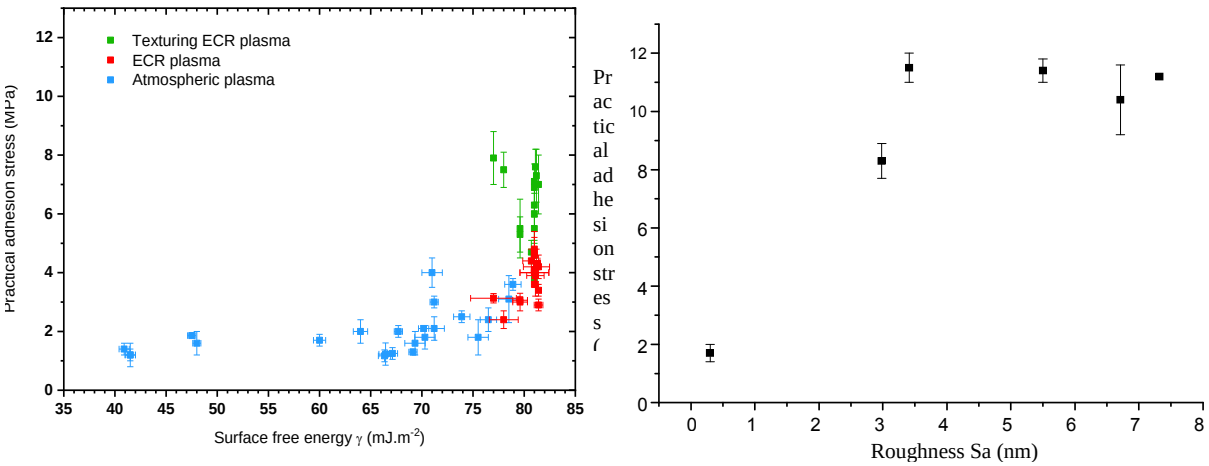

a) b)

Fig.12.

FIGURE 12. Dependence of practical adhesion stress a) of different assemblies on PEEK surface free energy; b) of textured assemblies on PEEK roughness

In the Figure 12a, it should be noticed that for textured ECR plasma samples, since the coherent contact angle measurements cannot be done, the reported surface free energy values of these samples correspond to those obtained on smooth samples in the same experimental conditions (power, pressure, plasma - surface distance and gas composition). The resulting plot highlights the effect of the texture added to the chemical functionalization in terms of adhesion. The measured practical adhesion stress increases from an interval of 2.5 to 5 MPa (non-textured surfaces) to an interval of 4 to 8 MPa (textured surfaces). This increase in the practical adhesion stress by a multiplying factor of 1.6 therefore clearly shows here the cumulative effect of the texture and of the chemical functionalization of the surface which can be added in the case of the low pressure plasma. Figure 12b illustrates the mechanical behavior of assemblies in the case of the textured PEEK on the roughness (*Sa*) as determined by AFM. Overall, the measured practical adhesion stress increases when the roughness also increases showing a certain correlation. However, a plateau is observed at around 11.5 MPa for all samples with a cohesive rupture, while the other assemblies have adhesive ruptures. Thus, practical adhesion stress is dependent on the roughness if the roughness does not exceed 30 nm; for denser texture, the rupture of PEEK due to mechanical failure becomes restraining. In conclusion, on Al-PEEK assembly, Figure 13 provides an overview on the balance between

the chemical (functionalization) and the texturing (mechanical anchoring) effects on a polymer surface using plasma and laser technologies. Polymer texturing is playing a major role towards the anchoring effect which can be associated with the chemical modification of the surface with only one process in the case of plasmas.

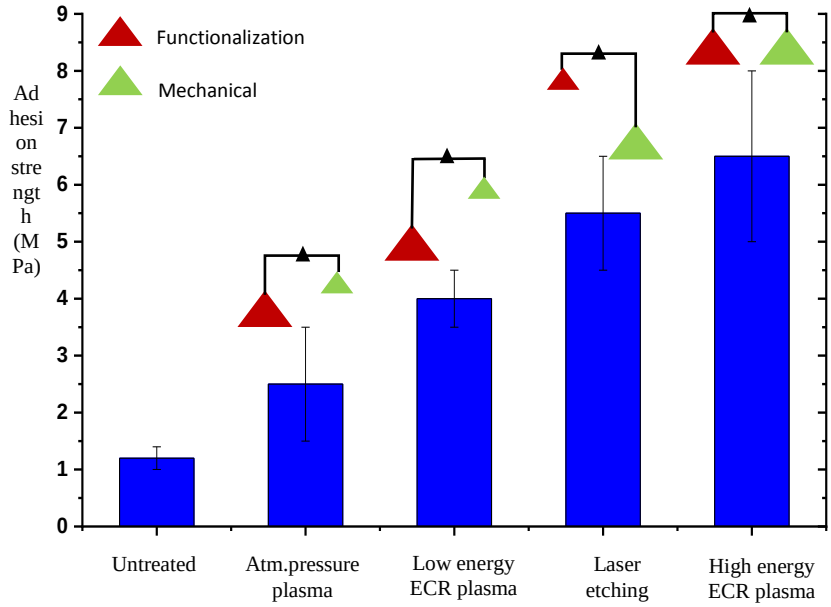

FIGURE 13. Competitive balance between the mechanical anchoring and the surface chemistry of modified PEEK in the case of different plasma treatments or laser texturing

4 CONCLUSION

Different types of surface treatments with laser irradiation and plasma processes were compared in order to prepare textured surfaces and to study the influence of the obtained pattern on the mechanical behavior of metal-polymer assemblies. The obtained results were also compared with plasma chemically modified surfaces. The laser ablation in static, then in a dynamic mode, gives rise to an increase in the width and depth of the structures, depending on the laser power and the pulse overlap. This study highlights the appearance of a random texture, of smaller scale than texturing lines, coming from thermal degradation of the surface and redeposition of material resulting in a clear improvement in the adhesion of thin Al layers. However, a two dense texturing pattern, which induces an increase in the specific surface, does not show an optimization of the adhesion. Indeed, an increase in the density of the patterns induces a higher rate of coverage by the random secondary structure. This

redeposited matter then forms a layer of low cohesion, weakening the assembly despite a significant increase in the roughness and the specific surface. The purely geometric criteria are not sufficient to explain all the adhesion phenomena. ECR plasma treatment with applying an external bias voltage also induces a surface patterning that increases the adhesion of the thin Al layer. Compared to Ar/N_2 or Ar/O_2, dioxygen plasma appears to be the most effective, followed by argon and dinitrogen plasmas. Furthermore, Ar plasma-texturing is mainly due to the atomization of matter by ion bombardment; thermal effects induce fusion and surface rearrangement. With N_2 plasma, an ion bombardment is always noticed, however, less intense, limiting thermal phenomena. Chemical degradation of the surface also takes place, preferentially eroding the amorphous phases of the material. O_2 plasmas are not dense enough to be as effective as an ion bombardment. Its texturing is therefore mainly due to the chemical degradation of the polymer into volatile or diffusing compounds towards the crystalline zones. The mode of rupture (adhesive or cohesive) is dependent on the type of treatment and on the experimental conditions, but the increase in the adhesion of the interface cannot be directly linked to an increase in surface roughness, as more parameters have to be considered.

AUTHOR CONTRIBUTIONS

David Gravis, Grégoire Rigolé, Mayssa Yengui, Wolfgang Knapp, Jean-François Coulon and Fabienne Poncin-Epaillard were involved in conceptualization, investigation, writing—original draft, project management. Jean-François Coulon and Fabienne Poncin-Epaillard. were involved in investigation, writing—review and editing.

CONFLICT OF INTEREST

The authors declare no financial or commercial conflict of interest.

DATA AVAILABILITY STATEMENT

The data that support the findings of this study are available from the corresponding author upon reasonable request.

REFERENCES

[1] A. J. Kinloch, *J. Mater. Sci.* **1980**, *15*, 2141.

[2] F. Awaja, M. Gilbert, G. Kelly, B. Fox, P. J. Pigram, *Prog. Polym. Sci.* **2009**, *34*, 948.

[3] G. Scarselli, · D. Quan, · N. Murphy, · B. Deegan, ·D. Dowling,· A. Ivankovic, Appl. Comp. Mat. **2021**, *28*, 71

[4] M. Gilliam, *Polymer Surface Treatment and Coating Technologies*, in: A.Y.C. Nee (Ed.), Handb. Manuf. Eng. Technol., Springer London, London, **2013**, 1.

[5] P. Blais, D.. Carlsson, G. Csullog, D.. Wiles, *J. Colloid Interface Sci.* **1974**, *47*, 636.

[6] J. Lawrence, L. Li, *Mater. Sci. Eng. A.* **2001**, *303*, 142.

[7] D. L. Pugmire, E.A. Waddell, R. Haasch, M. J. Tarlov, L. E. Locascio, Anal. Chem. **2002**, *74*, 871.

[8] H. Pazokian, A. Selimis, J. Barzin, S. Jelvani, M. Mollabashi, C. Fotakis, E. Stratakis, *J. Micromechanics Microengineering*. **2012**, *22*, 035001.

[9] Q. Du, J. Liu, L. Guo, M. Ly, X. Zeng, *Mater. Des.* **2016**, *104*, 134.

[10] Y. Kawamura, K. Toyoda, S. Namba, *Appl. Phys. Lett.* **1982**, *40*, 374.

[11] R. Srinivasan, V. Mayne- Banton, *Appl. Phys. Lett.* **1982**, *41*, 576.

[12] S. I. Anisimov, N. M. Bityurin, B. S. Luk'yanchuk, *Models for Laser Ablation, in: Photo-Excited Process. Diagnostics Appl.*, Kluwer Academic Publishers, Boston, **2003**, 121.

[13] B. J. Garrison, R. Srinivasan, *J. Appl. Phys.* **1985**, *57*, 2909.

[14] S. Lazare, V. Granier, *Laser Chem.* **1989**, *10*, 25.

[15] S. Chen, V. V Kancharla, Y. Lu, *Int. J. Mater. Prod. Technol.* **2003**, *18*, 457.

[16] M. A. Roberts, J. S. Rossier, P. Bercier, H. Girault, Anal. Chem. **1997**, *69*, 2035.

[17] E. Kostal, S. Stroj, S. Kasemann, V. Matylitsky, M. Domke, *Langmuir* **2018**, *34*, 2933.

[18] M. R. Hauer, *Laser ablation of polymers studied by time resolved methods, Degree Thesis*, Swiss federal institute of technology Zurich, **2004**.

[19] T. Lippert, A. Yabe, A. Wokaun, *Adv. Mater.* **1997**, *9*, 105.

[20] N. Arnold, N. Bityurin, *Indo-Pacific J. Phenomenol.* **2002**, *2*, 1.

[21] S. Küper, M. Stuke, *Appl. Phys. Lett.* **1989**, *54*, 4.

[22] A. A. Serafetinides, M. I. Makropoulou, C. D. Skordoulis, A. K. Kar, *Appl. Surf. Sci.* **2001**, *180*, 42.

[23] S. I. Bozhevolnyi, I. V. Potemkin, *J. Phys. D. Appl. Phys.* **1994**, *27*, 19.

[24] P. E. Dyer, R. Srinivasan, *Appl. Phys. Lett.* **1986**, *48*,445.

[25] C. Momma, S. Nolte, B. N. Chichkov, F. v. Alvensleben, A. Tünnermann, *Appl. Surf. Sci.* **1997**, *109–110* () 15.

[26] W.-S. Kim, I.-H. Yun, J.-J. Lee, H.-T. Jung, *Int. J. Adhes. Adhes.* **2010**, *30*, 408.

[27] Y. C. Jung, B. Bhushan, *Nanotechnology.* **2006**, *17*, 4970.

[28] R. Kromer, S. Costil, J. Cormier, D. Courapied, L. Berthe, P. Peyre, M. Boustie, *Surf. Coatings Technol.* **2015**, *278*, 171.

[29] D. Martina, C. Creton, P. Damman, M. Jeusette, A. Lindner, *Soft Matter.* **2012**, *8*, 5350.

[30] H. Qi, T. Chen, L. Yao, T. Zuo, *Microfluid. Nanofluidics.* **2008**, *5*, 139.

[31] J. S. Rossier, P. Bercier, A. Schwarz, S. Loridant, H. H. Girault, *Langmuir*. **1999**, *15*, 5173.

[32] W. Lee, M. K. Jin, W. C. Yoo, J. K. Lee, *Langmuir*. **2004,** *20*, 7665.

[33] S. E. More, P. S. Das, A. Bansode, G. Dhamale, S. Ghorui, S. V. Bhoraskar, S. N. Sahasrabudhe, V. L. Mathe, *Rev. Sci. Instrum.* **2018**, *89*, 013509.

[34] S. Wang, Y. Deng, L. Yang, X. Shi, W. Yang, ZG. Chen, *J. Biomat. Sci., Polym. Ed*. **2018**, *29*, 520.

[35] K. Du, Y. Jiang, PS. Huang, J. Ding, T. Gao, CH. Choi, J. Micromech. Microeng. **2018**, *28*, 014006.

[36] F. Palumbo, C. Lo Porto, P. Favia, Coatings **2019**, *9*, 640.

[37] P. Dimitrakellis, E. Gogolides, Microelec. Eng. **2018**, *194*, 109.

[38] R. Foerch, N. S. Mcintyre, R. N. S. Sodhi, D. H. Hunter, *J. Appl. Polym. Sci.* **1990**, *40*, 1903.

[39] M. J. Shenton, G. C. Stevens, N. P. Wright, X. Duan, *J. Polym. Sci. Part A Polym. Chem.* **2002**, *40*, 95.

[40] F. D. Egitto, L. J. Matienzo, *IBM J. Res. Dev.* **1994**, *38*, 423.

[41] S. A. Rich, T. Dufour, P. Leroy, L. Nittler, J. J. Pireaux, F. Reniers, *J. Phys. D. Appl. Phys.* **2014**, *47*, 065203.

[42] D.M. Choi, C.K. Park, K. Cho, C.E. Park, *Polymer*. **1997**, *38*, 6243.

[43] A. Vesel, I. Junkar, U. Cvelbar, J. Kovac, M. Mozetic, *Surf. Interface Anal.* **2008,** *40*,1444.

[44] G. Borcia, N. Dumitrascu, G. Popa, *Surf. Coatings Technol.* **2005**, *197*, 316.

[45] E. M. Liston, L. Martinu, M. R. Wertheimer, *J. Adhes. Sci. Technol.* **1993**, *7*,1091.

[46] G. Borcia, A. Chiper, I. Rusu, *Plasma Sources Sci. Technol.* **2006**, *15*, 849.

[47] F. Palumbo, R. Di Mundo, D. Cappelluti, R. D'Agostino, *Plasma Process. Polym.* **2011**, *8*, 118.

[48] C. Lambaré, P.-Y. Tessier, F. Poncin-Epaillard, D. Debarnot, *RSC Adv.* **2015**, *5*, 62348.

[49] R. Di Mundo, V. De Benedictis, F. Palumbo, R. D'Agostino, *Appl. Surf. Sci.* **2009**, *255*, 5461.

[50] A. Milella, R. Di Mundo, F. Palumbo, P. Favia, F. Fracassi, R. D'Agostino, *Plasma Process. Polym.* **2009**, 6, 460.

[51] K. Ellinas, K. Tsougeni, P.S. Petrou, G. Boulousis, D. Tsoukleris, E. Pavlatou, A. Tserepi, S.E. Kakabakos, E. Gogolides, *Chem. Eng. J.* **2016**, *300*, 394.

[52] D. Gravis, F. Poncin-Epaillard, J.F. Coulon, *Appl. Surf. Sci.* **2020**, *501*, 144242.

[53] D. K. Owens, R. C. Wendt, *J. Appl. Polym. Sci.* **1969**, *13*, 1741.

[54] D. Gravis, F. Poncin-Epaillard, J.-F. Coulon, *Plasma Process. Polym.* **2018**, *15*,

[55] J.F. Coulon, N. Tournerie, H. Maillard, *Appl. Surf. Sci.* **2013,** *283*, 843.

[56] S. Genty, J.-B. Sauvage, P. Tingaut, M. Aufray, *Int. J. Adhes. Adhes.* **2017**, *79*, 50.

[57] T. Lippert, *Laser-Surface Interact. New Mater. Prod.* **2010**, 141.

[58] T. Lippert, *Plasma Process. Polym.* **2005**, *2*, 525.

[59] B. C. Stuart, M. D. Feit, S. Herman, A. M. Rubenchik, B. W. Shore, M. D. Perry, *Phys. Rev. B.* **1996**, *53*, 1749.

[60] D. Zhang, F. Chen, Q. Yang, J. Si, X. Hou, *Soft Matter.* **2011**, *7*, 8337.

[61] L. Feng, S. Li, Y. Li, H. Li, L. Zhang, J. Zhai, Y. Song, B. Liu, L. Jiang, D. Zhu, *Adv. Mater.* **2002**, *14*, 1857.

[62] W. Knapp, V. Gillet, B. Courant, E. Aubignat, S. Costil, C. Langlade, Proc. SPIE - Int. Soc. Opt. Eng., **2017**, 100970.

[63] J. Tarrade, T. Darmanin, E. Taffin de Givenchy, F. Guittard, D. Debarnot, F. Poncin-Epaillard, *Appl. Surf. Sci.* **2014**, *292*, 782.

[64] A. Zaitsev, A. Lacoste, F. Poncin-Epaillard, A. Bès, D. Debarnot, *Surf. Coatings Technol.* **2017**, *330*, 196.

[65] K. L. L. Mittal, M. Thomas, Atmospheric Pressure Plasma Treatment of Polymers: Relevance to Adhesion, Wiley, 2013.

[66] F. Poncin-Epaillard, J.M. Herry, P. Marmey, G. Legeay, D. Debarnot, M.N. Bellon-Fontaine, *Mater. Sci. Eng. C.* **2013**, *33*, 1152.

[67] K. S. Siow, L. Britcher, S. Kumar, H. J. Griesser, *Plasma Process. Polym.* **2006**, *3*, 392.

[68] S. Espinho, S. Hofmann, J. M. Palomares, S. Nijdam, *Plasma Sources Sci. Technol.* **2017**, *26*, 105008.

[69] E. I. Toader, *Plasma Sources Sci. Technol.* **2004**, *13*, 646.

[70] N. Inagaki, K. Narushim, N. Tuchida, K. Miyazaki, *J. Polym. Sci. Part B Polym. Phys.* **2004**, *42* 3727.

[71] C. C. Dupont-Gillain, Y. Adriaensen, S. Derclaye, P. G. Rouxhet, *Langmuir.* **2000**, *16*, 8194.

[72] R. Morent, N. De Geyter, L. Gengembre, C. Leys, E. Payen, S. Van Vlierberghe, E. Schacht, *Eur. Phys. J. Appl. Phys.* **2008**, *43*, 289.

[73] J. M. Grace, L. J. Gerenser, *J. Dispers. Sci. Technol.* **2003**, *24*, 305.

[74] I. Mathieson, R. H. Bradley, *Int. J. Adhes. Adhes.* **1996**, *16*, 29.

[75] N. Inagaki, S. Tasaka, K. Hibi, *J. Adhes. Sci. Technol.* **1994**, *8*, 395.

[76] R. J. Good, *J. Adhes.* **1972**, *4*, 133.

Table of contents

This paper deals with the dependence of metal – polymer assembly on mechanical anchoring. The influence of ECR, AP plasmas and laser texturing on Al adhesion on PEEK was demonstrated. It appears that the O_2 ECR plasma is the most efficient for texturing and chemical functionalization.

Graphic